Chemical Engineering Journal 518 (2025) 164657

Contents lists available at ScienceDirect

Chemical Engineering Journal

journal homepage: www.elsevier.com/locate/cej

Polymersomal vincristine-PLK1 inhibitor boosts immunogenic cell death and antitumor immunity

Yan Zhao [a], Li Cao [b], Songsong Zhao [a], Zhenzhen Zhai [a], Xueling Tang [a], Lin Chen [a], Huanli Sun [a,*], Zhiyuan Zhong [a,b,c,**]

[a] State Key Laboratory of Bioinspired Interfacial Materials Science, and Biomedical Polymers Laboratory, College of Chemistry, Chemical Engineering and Materials Science, Soochow University, Suzhou 215123, PR China
[b] College of Pharmaceutical Sciences, Soochow University, Suzhou 215123, PR China
[c] International College of Pharmaceutical Innovation, Soochow University, Suzhou 215222, PR China

ARTICLE INFO

Keywords:
Cancer immunotherapy
Drug delivery
Nanomedicines
PD-1 blockade
Synergistic therapy

ABSTRACT

Cancer immunotherapy has achieved remarkable progress in cancer treatment. However, its clinical efficacy in solid tumors remains limited, likely due to the immunosuppressive tumor microenvironment (TME). Immunogenic cell death (ICD) holds great promise for regulating the TME and enhancing antitumor immunity; however, ICD inducers such as chemotherapy and radiotherapy typically lack specificity and can cause harmful effects on the immune system. Herein, we report a safe and potent ICD nanoinducer based on dual-drug polymersomes incorporating vincristine and the polo-like kinase 1 inhibitor volasertib (NanoVi/Vo) to boost immunotherapy in solid tumors. NanoVi/Vo synergistically induces ICD while causing apoptosis in cancer cells and facilitates dendritic cell maturation, T cell activation and infiltration, effectively reversing the immunosuppressive TME. NanoVi/Vo significantly increased the cure rate in subcutaneous 4T1 breast cancer and MC38 colorectal cancer as well as in postoperative 4T1 models, particularly when combined with anti-PD-1 treatment, with > 57 % of the mice becoming tumor free. This potent ICD nanoinducer offers great promise for augmenting immunotherapy in solid tumors.

1. Introduction

Cancer immunotherapy has revolutionized the treatment paradigm of diverse malignancies by leveraging the intrinsic immune system to combat cancer [1–4]. For example, immune checkpoint blockade (ICB) and adoptive cell therapy have achieved significant progress in treating hematological cancers; however, their clinical efficacy in solid tumors such as triple-negative breast cancer (TNBC) and colorectal cancers remains limited [5–8]. One of the main underlying factors lies in the immunosuppressive tumor microenvironment (TME), which is characterized by the poor infiltration of immune cells, particularly T cells [9–11].

One promising TME-modulating approach is the induction of immunogenic cell death (ICD) in cancer cells, which can increase immunogenicity via the release of damage-associated molecular patterns (DAMPs), the stimulation of dendritic cells (DCs), and the promotion of T cell activation and infiltration [12–16]. Chemotherapy and molecular targeted therapy, two critical strategies in cancer treatment, have been shown to induce ICD while killing cancer cells and reverse the immunosuppressive TME [17–20]. However, these small-molecule drugs typically have low delivery efficiency to cancer cells along with serious harmful effects on the immune system, which may largely limit the ICD effects and the antitumor immune response [21,22]. In addition, the propensity of developing resistance also restricts the ICD effects induced by single-drug treatment.

In this study, we developed a potent ICD nanoinducer based on the polymersomal vincristine-PLK1 inhibitor volasertib (NanoVi/Vo) to synergistically induce ICD while king cancer cells, thereby potentiating immunotherapy in solid tumors (Fig. 1A). PLK1, which has oncogenic properties, is overexpressed in various malignancies and is correlated not only with drug resistance and an inferior prognosis but also with an immunosuppressive TME [23,24]. PLK1 inhibition has emerged as an

* Corresponding author.
** Corresponding author at: State Key Laboratory of Bioinspired Interfacial Materials Science, and Biomedical Polymers Laboratory, College of Chemistry, Chemical Engineering and Materials Science, Soochow University, Suzhou 215123, PR China.
E-mail addresses: sunhuanli@suda.edu.cn (H. Sun), zyzhong@suda.edu.cn (Z. Zhong).

https://doi.org/10.1016/j.cej.2025.164657
Received 21 April 2025; Received in revised form 1 June 2025; Accepted 7 June 2025
Available online 10 June 2025

effective antitumor therapeutic strategy, with several PLK1 inhibitors, including Vo, having advanced to clinical trials for the treatment of different cancers [25,26]. One recent report revealed that PLK1 inhibition can induce ICD in lung cancer cells and enhance antitumor immunity [27]. Moreover, preliminary cellular studies have shown that Vi and Vo have strong synergistic effects on the induction of cancer cell apoptosis [28]. NanoVi/Vo can facilitate ratiometric delivery of Vi and Vo to cancer cells, maximizing synergistic effects in vivo. Notably, the NanoVi/Vo ICD inducer synergistically induced apoptosis and ICD in various cancer cells, thereby promoting DC maturation, T cell activation and infiltration in a 4T1 TNBC model. This consequently boosted immunotherapy in the 4T1 TNBC and MC38 colorectal cancer models, and cooperation with the anti-PD-1 antibody (aPD-1) further enhanced the efficacy, leading to complete tumor eradication in 57.1–62.5 % of the mice. Furthermore, fibrin gel-mediated local delivery of NanoVi/Vo and aPD-1 effectively inhibited tumor recurrence and lung metastasis in the postoperative 4T1 model.

2. Results and discussion

2.1. Preparation of a dual-drug polymersome-based ICD nanoinducer (NanoVi/Vo)

Considering the high water solubility of vincristine sulfate (Vi) and

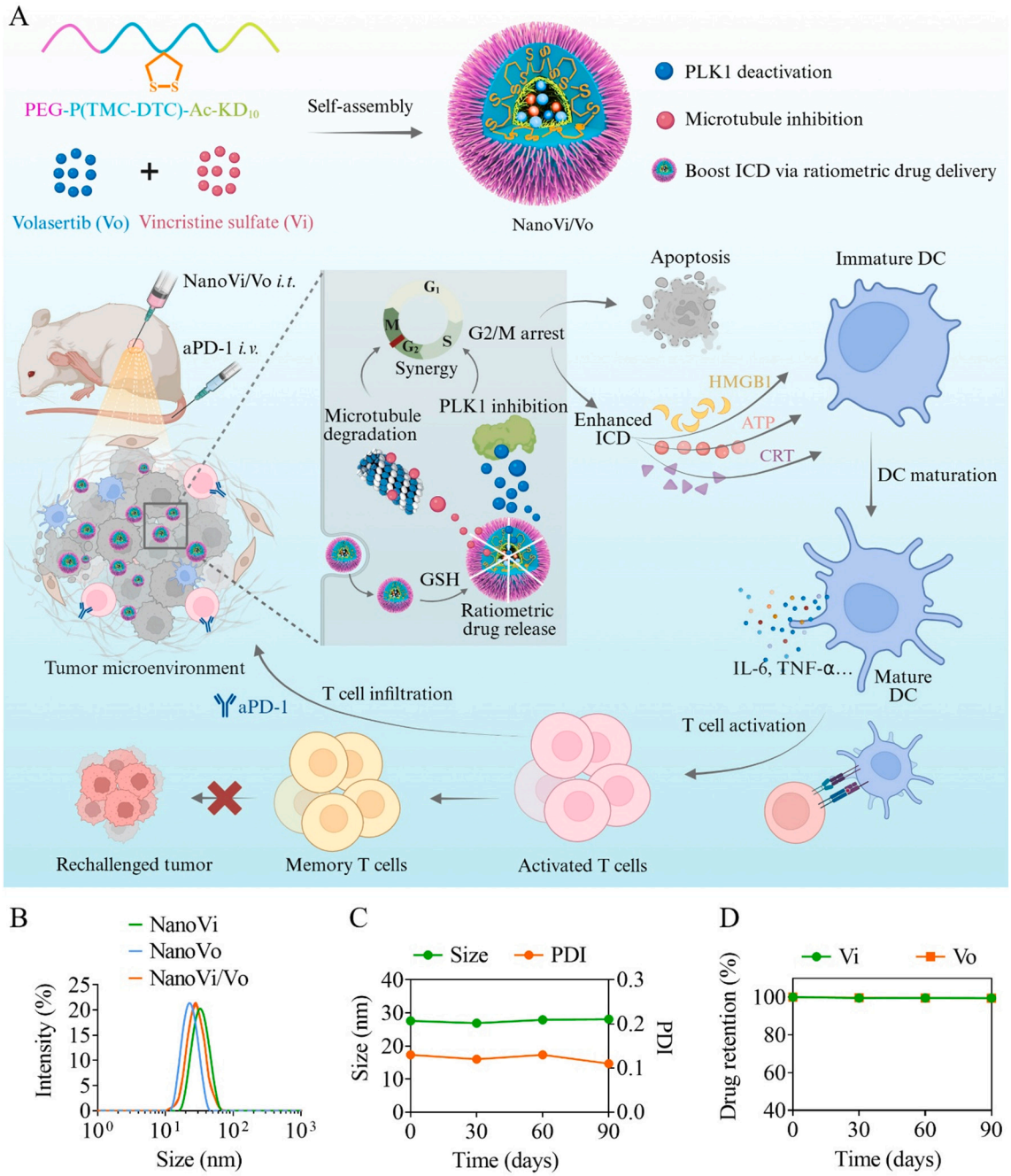

Fig. 1. Fabrication of a polymersomal vincristine/volasertib (NanoVi/Vo)-based ICD nanoinducer for enhancing immunotherapy and characterization of NanoVi/Vo. (A) Schematic showing the preparation of NanoVi/Vo as an ICD nanoinducer to cooperate with aPD-1 to enhance immunotherapy. (B) Size distributions of NanoVi, NanoVo and NanoVi/Vo measured by dynamic light scattering (DLS). (C) Size and PDI variation and (D) drug retention of NanoVi/Vo during 90 days of storage at 4 °C.

the amphipathy of volasertib (Vo) along with their positively charged nature, chimeric polymersomes with a negatively charged cavity were prepared via one-step self-assembly of amphiphilic poly(ethylene glycol)-*b*-poly(trimethylene carbonate-*co*-dithiolane trimethylene carbonate)-*b*-*N*-acetylated poly(aspartic acid) (PEG-P(TMC-DTC)-Ac-KD_{10}, 5.0-(15.0-2.0)-1.3 kg/mol), which was synthesized according to our previous report [29]. These chimeric polymersomes enabled effective coencapsulation of Vi and Vo through electrostatic interactions, resulting in dual-drug polymersomes (NanoVi/Vo) with a Vi/Vo mass ratio of ca. 1:24. NanoVi/Vo had a small size of ca. 27.8 nm, which is between those of NanoVi (32.6 nm) and NanoVo (22.3 nm), and a narrow size distribution with a polydispersity index below 0.1 (Fig. 1B and Table S1). Moreover, compared with single drug polymersomes, NanoVi/Vo demonstrated a similar loading efficiency for Vo but a lower loading efficiency for Vi, likely due to the lower feeding amount of Vi and charge competition between the two drugs. Notably, NanoVi/Vo displayed excellent stability during 90 days of storage at 4 °C; specifically, its size and size distribution were consistently maintained, and drug leakage was < 1 % (Fig. 1C, D). In addition, NanoVi/Vo maintained its physical appearance and retained an intact polymersome structure after long-term storage (Fig. S1).

2.2. *In vitro synergistic antitumor effects, ICD induction and PD-L1 modulation of NanoVi/Vo*

The synergistic antitumor effects of NanoVi/Vo were evaluated via an MTT assay using breast and colorectal cancer cell lines (4T1, MC38 and CT26). On the basis of the half-maximal inhibitory concentration (IC_{50}) values of NanoVi/Vo and single-drug formulations (NanoVi and NanoVo), the combination index (CI) was calculated to assess the synergistic effects of NanoVi/Vo. Specifically, CI < 1 signifies a synergistic effect, CI = 1 indicates an additive effect, and CI > 1 suggests an antagonistic effect. In 4T1 TNBC cells, NanoVi/Vo effectively inhibited cell proliferation and exhibited IC_{50} values of 2.2 and 53.6 ng/mL for Vi and Vo, respectively, which were 11.7 and 4.3-fold lower than those of NanoVi (29.3 ng/mL) and NanoVo (228 ng/mL), respectively (Fig. 2A). This consequently resulted in a low CI value of 0.32, suggesting a robust synergistic antitumor effect of NanoVi/Vo. Similarly, NanoVi/Vo also elicited significantly lower IC_{50} values in MC38 (Vi/Vo: 2.0/49.4 ng/mL) and CT26 (Vi/Vo: 3.8/90.7 ng/mL) colorectal cancer cells than did NanoVi and NanoVo, leading to strong synergistic effects with CI values of 0.31 and 0.58, respectively (Fig. 2B, S2). Vi is reported to block tubulin polymerization and trigger mitotic arrest, thus causing cell apoptosis [30–32]. Vo has also been shown to cause mitotic arrest and subsequent apoptosis via PLK1 inhibition [33–35]. We therefore investigated the synergistic proapoptotic ability of NanoVi/Vo using an Annexin V/7-AAD kit. As shown in Fig. 2C, D, NanoVi/Vo provoked the highest level of apoptosis in 4T1 cells, with 49.4 % of cells in the early stages of apoptosis and 23.8 % in the late stages, which were markedly greater than those observed in cells treated with NanoVi (17.9 % and 7.7 %) or NanoVo (26.3 % and 9.0 %). A similar tendency was also observed in MC38 cells (Fig. 2E, S3).

Certain molecular targeted drugs, such as the tyrosine kinase inhibitor crizotinib and the proteasome inhibitor bortezomib, have been shown to induce ICD in tumor cells, thus facilitating antigen presentation and activating the antitumor immune response [36,37]. One recent study also demonstrated the potential of PLK1 inhibition in inducing ICD in lung cancer cells [27]. Herein, the synergistic ICD effect of NanoVi/Vo was investigated in 4T1 and MC38 cells via detection of typical ICD markers (CRT, ATP and HMGB1). Compared with PBS treatment, NanoVo treatment significantly increased CRT exposure and ATP release in both 4T1 and MC38 cells. This effect was further enhanced substantially in NanoVi/Vo-treated cells, which was in sharp contrast to the negligible effect of NanoVi. For example, NanoVi/Vo treatment of 4T1 cells induced 32.1 % CRT-positive cells, which was significantly greater than that of NanoVi (10.2 %), NanoVo (18.8 %), and PBS (4.8 %), resulting in markedly greater CRT median fluorescence intensity (MFI) (Fig. 2F, S4A). Moreover, compared with the other control treatments, NanoVi/Vo treatment noticeably increased ATP and HMGB1 levels in the culture medium of 4T1 cells (Fig. 2G, S4B). Similarly, NanoVi/Vo effectively enhanced membrane CRT exposure and promoted the secretion of ATP and HMGB1 in MC38 cells, which was greater than that in all the controls (Fig. 2H, I, S5).

The DAMPs released during ICD can be captured by antigen-presenting cells, such as DCs, to promote their maturation and presentation to T cells, thus activating the immune response [38–40]. To determine the degree of DC maturation stimulated by the ICD effect, BMDCs were cultured with drug-treated tumor cells for 24 h and then analyzed by flow cytometry (Fig. 2J). NanoVi/Vo-treated 4T1 cells increased the proportion of mature DCs ($CD80^+CD86^+$) from 8.5 % in the PBS group to 21.5 %, which was significantly higher than that in the NanoVi and NanoVo groups (Fig. 2K, L). Moreover, the level of the proinflammatory cytokine IL-6 in the medium was significantly elevated in the NanoVi/Vo group (Fig. 2M). Consistently, NanoVi/Vo-treated MC38 cells also substantially increased the maturation of DCs to 34 % and promoted the secretion of the proinflammatory cytokine TNF-α compared with all the other control groups (Fig. 2N, O, S6). Taken together, NanoVi/Vo not only synergistically inhibited tumor cell proliferation but also induced pronounced ICD effects, which effectively facilitated the maturation of DCs and the secretion of proinflammatory cytokines.

In addition to their ICD effects, some chemotherapeutics and small molecule inhibitors can also upregulate PD-L1 expression in tumor cells, which may diminish the function of cytotoxic T cells [41–43]. For example, one previous report demonstrated that Vo could upregulate PD-L1 expression on the membrane of lung cancer cells [24]. Therefore, we further explored the influence of NanoVi/Vo on PD-L1 expression in MC38 and 4T1 cells. The results revealed time-dependent PD-L1 upregulation in MC38 cells after treatment with NanoVo (Fig. S7A). Moreover, the PD-L1 upregulation induced by NanoVi/Vo in both 4T1 and MC38 cells was comparable to the effects observed with NanoVo and clearly occurred in a dose-dependent manner (Fig. 2P, Q). However, NanoVi had a negligible effect on PD-L1 expression at Vi concentrations ranging from 0.65 to 10.6 ng/mL (Fig. S7B). These findings indicate the potential of further combination of NanoVi/Vo with PD1/PD-L1 blockade to enhance antitumor immune responses.

2.3. *The combination of NanoVi/Vo and aPD-1 depletes tumors in 4T1 TNBC-bearing mice*

Motivated by our findings that NanoVi/Vo can induce a synergistic antitumor response, pronounced ICD effects and PD-L1 upregulation in tumor cells, we further evaluated the antitumor efficacy of NanoVi/Vo in combination with aPD-1 in syngeneic murine tumor models. An immunologically “cold” subcutaneous murine 4T1 TNBC model was first established for evaluation. The biodistribution and tumoral retention of NanoVi/Vo were first evaluated via in vivo fluorescence imaging using Cy5-labeled polymersomes (Nano-Cy5) when the tumors reached approximately 150–200 mm^3. After intratumor injection, Nano-Cy5 exhibited strong and prolonged retention within the tumor site (Fig. S8). This is in contrast to the rapid clearance of free Cy5, resulting in a pronounced decrease in tumoral Cy5 signals at 4 h post-injection. The mice were randomly grouped when the tumors reached an approximate volume of ca. 50–100 mm^3 and treated with PBS, NanoVi, NanoVo, NanoVi/Vo, aPD-1, or NanoVi/Vo&aPD-1 at Vi, Vo and aPD-1 dosages of 0.25, 6 and 1 mg/kg, respectively (Fig. 3A). As shown in Fig. 3B-D, NanoVi and NanoVo treatment only modestly inhibited tumor growth, and the median survival time (MST) of the mice was prolonged by only 11.5 or 8.5 days compared with that of the PBS group (MST: 18.5 days). In sharp contrast, treatment with NanoVi/Vo dual-drug polymersomes substantially inhibited tumor growth and significantly prolonged the survival of the mice, with 3 out of 8 mice becoming tumor

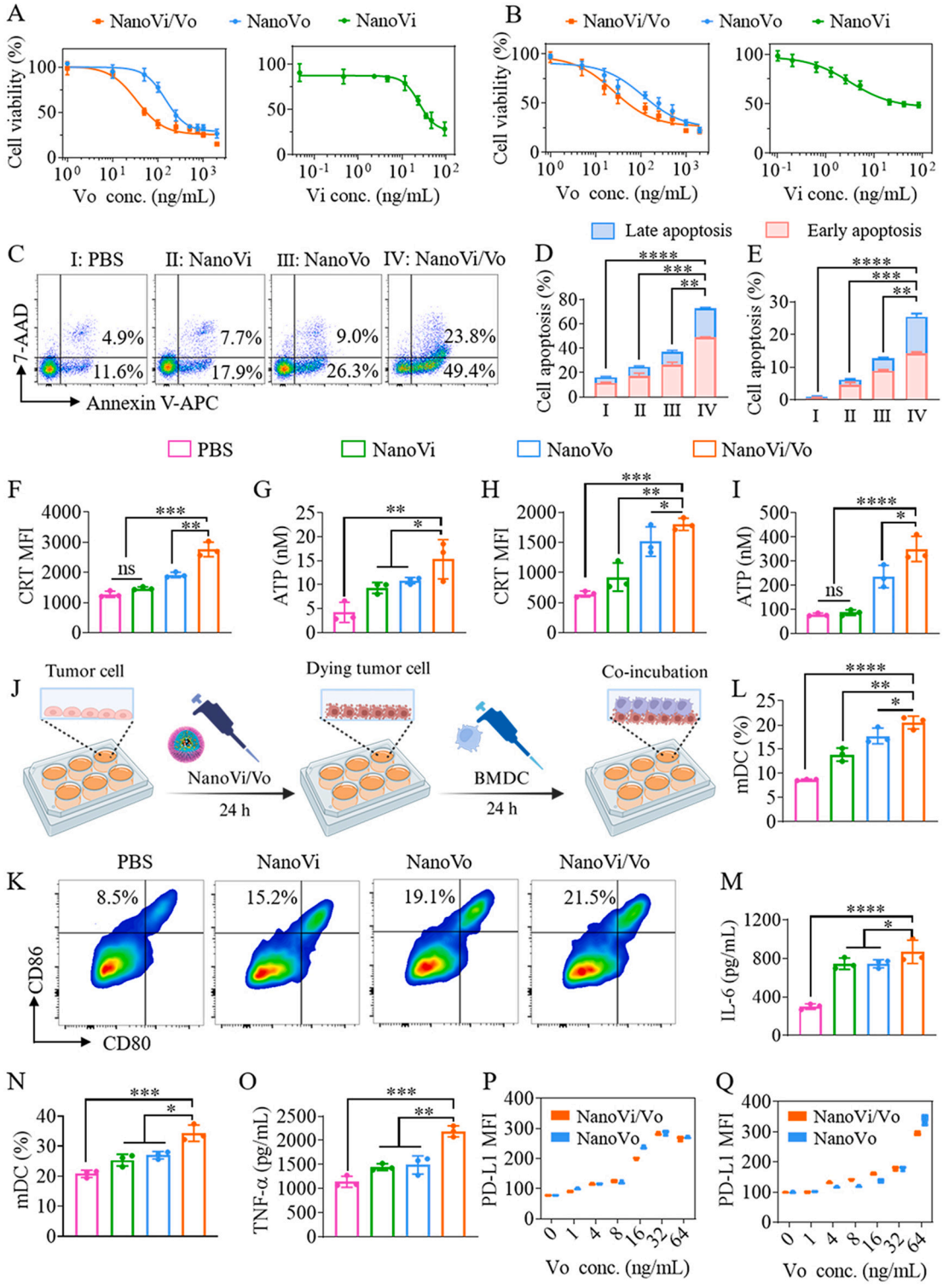

Fig. 2. Synergistic antitumor efficacy and ICD induction of NanoVi/Vo in vitro. PBS, NanoVi, and NanoVo were used as controls. Cytotoxicity of NanoVi/Vo, NanoVo and NanoVi toward (A) 4T1 cells and (B) MC38 cells ($n = 6$). (C) Representative flow cytometry patterns and (D) quantification of apoptotic 4T1 cells after 48 h of incubation with different formulations ($n = 3$). (E) Apoptosis analysis of MC38 cells after 48 h of incubation with PBS, NanoVi, NanoVo or NanoVi/Vo ($n = 3$). (F) Membrane CRT exposure and (G) ATP release in 4T1 cells treated with NanoVi/Vo or control formulations for 48 h ($n = 3$). (H) Membrane CRT exposure and (I) ATP release in MC38 cells treated with different formulations for 48 h ($n = 3$). (J) Schematic showing the study of tumor cell ICD-mediated BMDC maturation. (K) Representative flow cytometry patterns and (L) quantitative analysis of BMDC maturation and (M) IL-6 secretion after coculturing BMDCs with 4T1 cells pretreated with PBS, NanoVi, NanoVo or NanoVi/Vo for 24 h (n = 3). (N) Maturation and (O) TNF-α secretion of BMDCs following 24 h of incubation with drug-treated MC38 cells (n = 3). PD-L1 levels on the surface of (P) 4T1 and (Q) MC38 cells after incubation with NanoVo or NanoVi/Vo for 48 h (n = 3). *$p < 0.05$, **$p < 0.01$, ***$p < 0.001$, ****$p < 0.0001$.

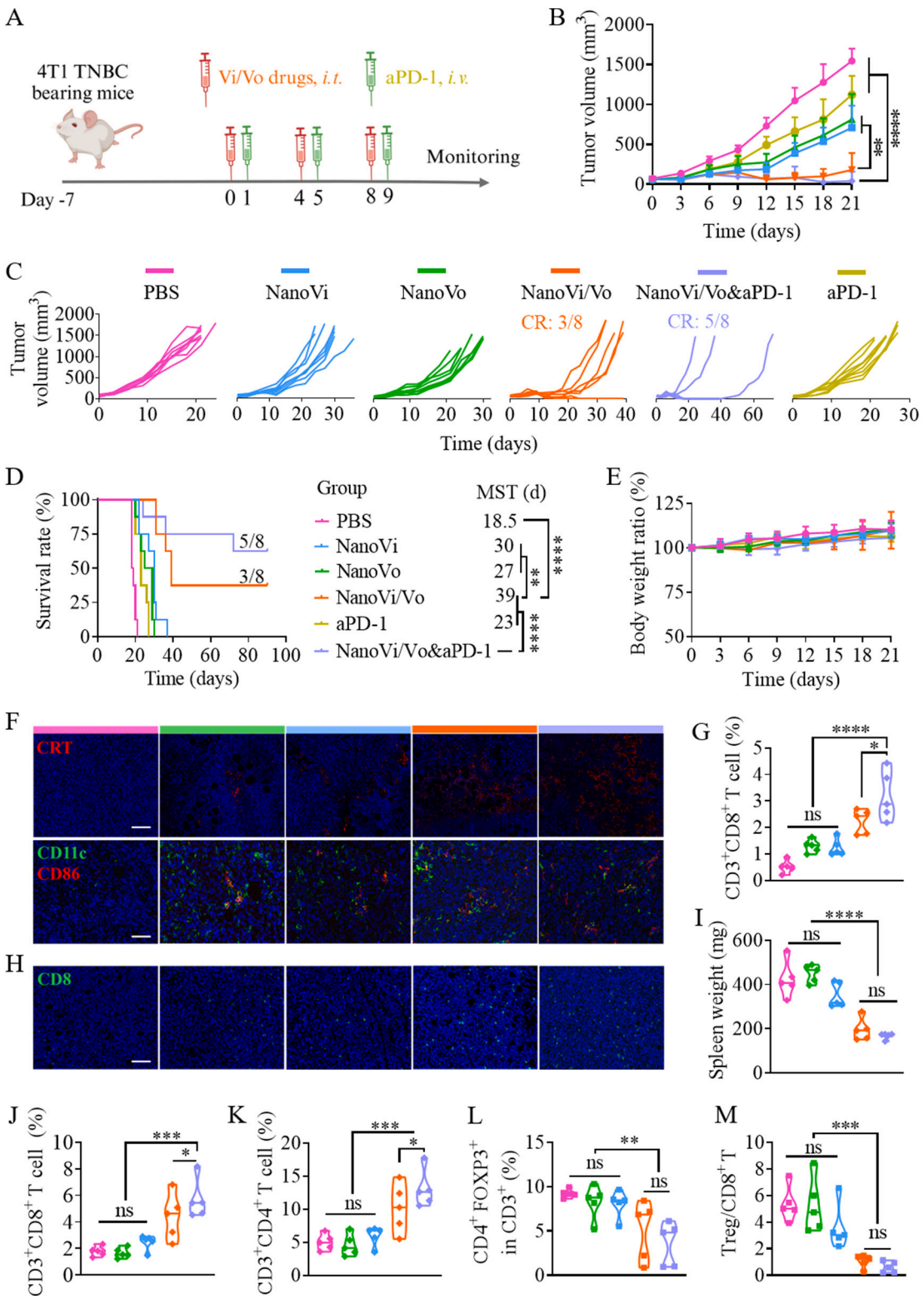

Fig. 3. In vivo therapeutic effects of NanoVi/Vo in combination with aPD-1 in a subcutaneous 4T1 TNBC model. PBS, NanoVi, NanoVo, NanoVi/Vo and aPD-1 were utilized as controls. (A) Schematic showing the treatment schedule. (B) Average and (C) individual tumor growth curves following different treatments ($n = 8$). (D) Survival curves and (E) body weight changes of the mice in different groups (n = 8). (F) Immunofluorescence images of tumor slices showing the CRT exposure and $CD11c^+CD86^+$ mDCs (scale bars: 40 μm). (G) Percentage of $CD3^+CD8^+$ T cells in tumors ($n = 5$). (H) Immunofluorescence images of tumor slices showing $CD8^+$ T cells (scale bars: 40 μm). (I) Weights of the spleens and the proportions of (J) $CD3^+CD8^+$ T cells, (K) $CD3^+CD4^+$ T cells, (L) Tregs and (M) the ratio of Treg/$CD8^+$ T cells in the spleen (n = 5). $^*p < 0.05$, $^{**}p < 0.01$, $^{***}p < 0.001$, $^{****}p < 0.0001$.

free and alive at the end of the observation period (90 days). Notably, the combination of NanoVi/Vo with aPD-1 further augmented the tumor inhibition effect, with 5 out of 8 mice being cured. However, aPD-1 monotherapy had limited therapeutic effects. H&E staining further confirmed the most extensive tumor cell shrinkage and apoptosis in the NanoVi/Vo&aPD-1-treated mice, whereas no apparent damage was observed in the normal organs (Fig. S9). Additionally, the body weights of the mice in all the groups steadily increased throughout the treatment period (Fig. 3E), and no obvious toxic effects were observed in the cured mice during the long-term observation period of 90 days.

To elucidate the potential underlying reasons, a subcutaneous 4T1 model was further established to evaluate the ICD effects and the immune response of different groups in vivo. NanoVi/Vo was injected twice with two injections of aPD-1. At 6 h after the last injection of aPD-1, blood samples were collected to analyze the plasma concentrations of TNF-α and IL-6, and tumors and spleens were collected at 24 h to analyze immune cells. Immunofluorescence images of tumor slices verified that the highest numbers of CRT-positive cells and $CD11c^+CD86^+$ mDCs were present in the NanoVi/Vo and NanoVi/Vo&aPD-1 treated groups (Fig. 3F), indicating the ICD effect and DC maturation in vivo. The infiltration of cytotoxic T lymphocytes (CTLs) into tumors is a prerequisite for activating antitumor immune responses [44]. Flow cytometry analysis revealed that the number of $CD8^+$ T cells in tumors treated with NanoVi/Vo was 4.6-fold greater than that in the PBS group, which was also significantly greater than that in the NanoVi or NanoVo treated tumors (****p) (Fig. 3G). Notably, the NanoVi/Vo&aPD-1 combination treatment further significantly enhanced the infiltration of $CD8^+$ T cells, the proportion of which was 6.4-fold higher than that in the PBS group. Fig. 3H further confirmed that the highest infiltration of $CD8^+$ T cells in the tumor site after treatment with NanoVi/Vo&aPD-1. The spleen is a crucial immune organ where lymphocytes encounter and engage with homologous antigens to initiate the immune response. Consequently, we further analyzed the T-cell population in the spleen. Consistent with the treatment trends, splenomegaly, a typical hallmark of the 4T1 tumor model [45,46], was significantly relieved after treatment with NanoVi/Vo in combination with aPD-1, resulting in much lower weights of the spleens than those in the other groups (Fig. 3I). The NanoVi/Vo&aPD-1 combination increased the percentages of $CD3^+CD8^+$ T cells and $CD3^+CD4^+$ T cells in the spleen to 5.6 % and 13.0 %, respectively, which were significantly greater than those in the NanoVi/Vo group and all the other control groups (Fig. 3J, K, S10). Moreover, the percentage of Tregs ($CD4^+FOXP3^+$) that weakened CTLs and the ratio of Treg/$CD8^+$ T cells were drastically decreased by the combination treatment (Fig. 3L, M). The ELISA results revealed that NanoVi/Vo in combination with aPD-1 effectively stimulated the production of IL-6 and TNF-α (Fig. S11), which are key proinflammatory cytokines in the antitumor immune response.

To assess the immune memory effect, the mice that had been cured in the NanoVi/Vo group ($n = 3$) and NanoVi/Vo&aPD-1 group ($n = 5$) were rechallenged with 4T1 cells on the contralateral side on day 76 (Fig. 4A). As shown in Fig. 4B, all the mice in the rechallenged group exhibited significantly slower growth of contralateral tumors than did the control healthy mice inoculated with an equal number of 4T1 cells. Furthermore, the weights of the spleens in the rechallenged groups were significantly lower than those in the control group (Fig. 4C). Flow cytometry analysis revealed that the percentages of $CD44^+CD62L^-$ Tem and $CD44^+CD62L^+$ Tcm cells among $CD4^+$ T cells in the peripheral blood of rechallenged mice significantly increased to approximately 21.5 % and 36.6 %, respectively, along with considerable increases in Tem and Tcm cells among $CD8^+$ T cells (Fig. 4D). Similarly, compared with control mice, rechallenged mice presented increased proportions of $CD4^+$ and $CD8^+$ Tem and Tcm cells in the spleen (Fig. 4E). Moreover, the ratios of Tregs to $CD8^+$ T cells in the spleens of rechallenged mice were also markedly reduced (Fig. S12). These results demonstrated that the

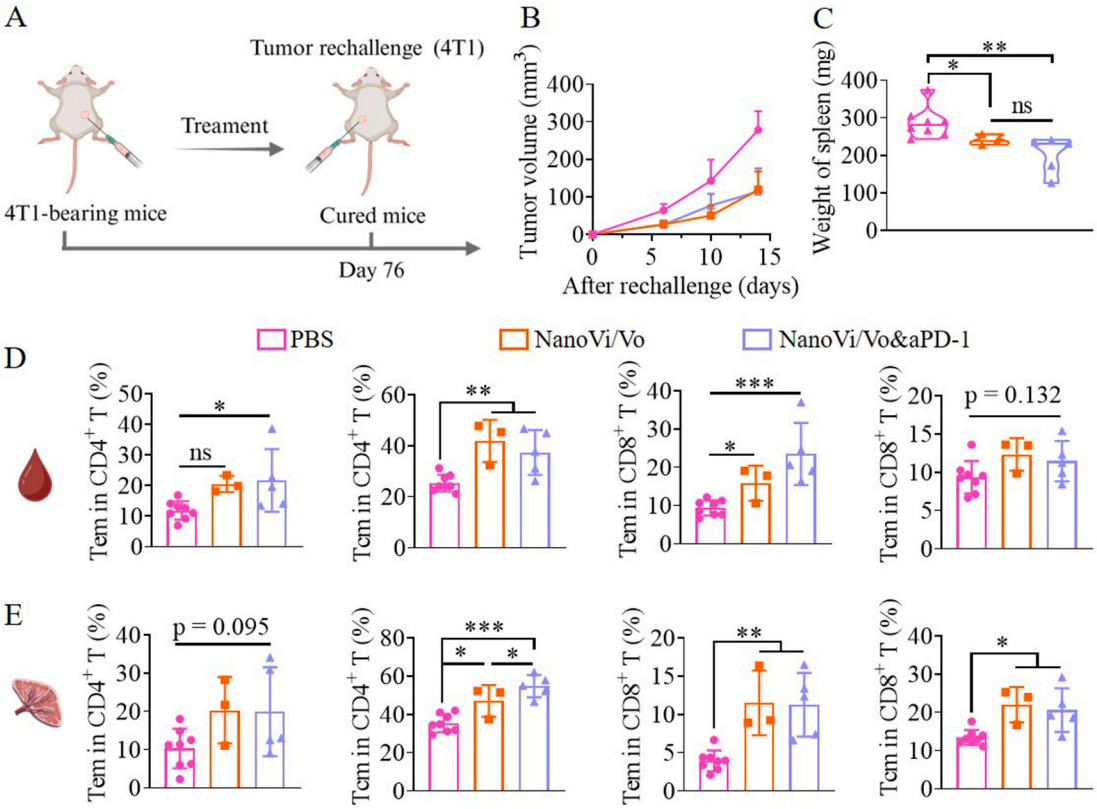

Fig. 4. The immune memory effects of NanoVi/Vo ($n = 3$) and NanoVi/Vo&aPD-1 ($n = 5$). Healthy mice inoculated with 4T1 cells were utilized as controls. (A) Schematic illustration of the rechallenge experiment. (B) Average tumor volume curves and (C) spleen weights. Proportions of Tem and Tcm in $CD8^+$ T cells and $CD4^+$ T cells in the (D) peripheral blood and (E) spleen. *$p < 0.05$, **$p < 0.01$, ***$p < 0.001$.

combination of NanoVi/Vo with PD-1 could effectively induce ICD, reverse the immunosuppressive microenvironment and stimulate anti-tumor immune memory effects.

2.4. The combination of NanoVi/Vo and aPD-1 depletes tumors in MC38 CRC-bearing mice

The therapeutic effect of NanoVi/Vo in combination with aPD-1 was further evaluated in a subcutaneous murine MC38 CRC model via the same treatment schedule and drug dosages as those used in the 4T1 model (Fig. 5A). As shown in Fig. 5B-D, NanoVi/Vo treatment effectively inhibited tumor growth and significantly prolonged the survival of the mice, with 1 out of the 7 mice becoming tumor free and alive at the end of the observation period (132 days), in contrast to the PBS, NanoVi and NanoVo control groups, whose MST was 18–25 days. aPD-1 monotherapy displayed limited therapeutic effects, with an MST of 22 days. Notably, the combination of NanoVi/Vo with aPD-1 exhibited a potent tumor inhibitory effect, with 4 out of 7 mice being cured and alive without tumors after 132 days. Additionally, the body weights of the mice in all the groups remained stable (Fig. 5E).

2.5. Postsurgical treatment in the mouse 4T1-Luc TNBC model

To further demonstrate the combination effect of NanoVi/Vo and aPD-1 in a postoperative tumor model, an in situ-forming fibrin gel containing both NanoVi/Vo and aPD-1 (NanoVi/Vo&aPD-1@Gel) was prepared and sprayed into the resection cavity of an incompletely resected 4T1-Luc TNBC model (Fig. 6A). The FDA-approved fibrin gel has been widely utilized for localized drug delivery in postsurgical settings [47,48]. We first prepared NanoVi/Vo&aPD-1@Gel by simply mixing a fibrinogen solution containing NanoVi/Vo and aPD-1 with thrombin solution (Fig. S13A). Rheology tests revealed that the storage modulus (G') of NanoVi/Vo&aPD-1@Gel was slightly greater than that of the blank gel (denoted Gel) (Fig. 6B), which is consistent with previous reports that doping nanoparticles increased gel elasticity [49–51]. The porous microstructure of NanoVi/Vo&aPD-1@Gel was confirmed via cold field emission scanning electron microscopy (FESEM) (Fig. S13B). The gel gradually degraded within two weeks (Fig. 6C), enabling the sustained release of the polymersomes and aPD-1 in PBS. Specifically, the polymersomes were released sustainably over 8 days, whereas aPD-1 was completely released within 52 h (Fig. 6D).

In vivo treatment was initiated when the tumors reached 200–300 mm^3. The mice were randomly grouped and subjected to incomplete surgical tumor resection, followed by spraying with Gel, NanoVi/Vo@Gel or NanoVi/Vo&aPD-1@Gel (Vi: 0.5 mg/kg, Vo: 12 mg/kg, aPD-1: 2 mg/kg) at the resection site with subsequent wound suturing (Fig. 6E). The day was designated day 0, and one group of mice with only surgical tumor resection was used as a control. Tumor growth was continuously monitored by detecting the bioluminescence signals of 4T1-Luc cells via an IVIS spectrum imaging system and calipers (Fig. 6F-H). The tumors recurred and grew rapidly in the untreated and Gel-treated groups, and the mice all died within one month. Spaying NanoVi/Vo@Gel significantly inhibited the growth of recurrent tumors, with 2 out of 6 mice achieving a complete cure and showing no detectable tumors. Intriguingly, NanoVi/Vo&aPD-1@Gel treatment improved the tumor inhibition and remission rates further, with 6 out of 8 mice becoming tumor free. Accordingly, 75 % of the mice in the NanoVi/Vo&aPD-1@Gel group survived for > 120 days, which was significantly better than that in the NanoVi/Vo@Gel group, with 33 % of the mice alive, and the other control groups, with no mice living for >

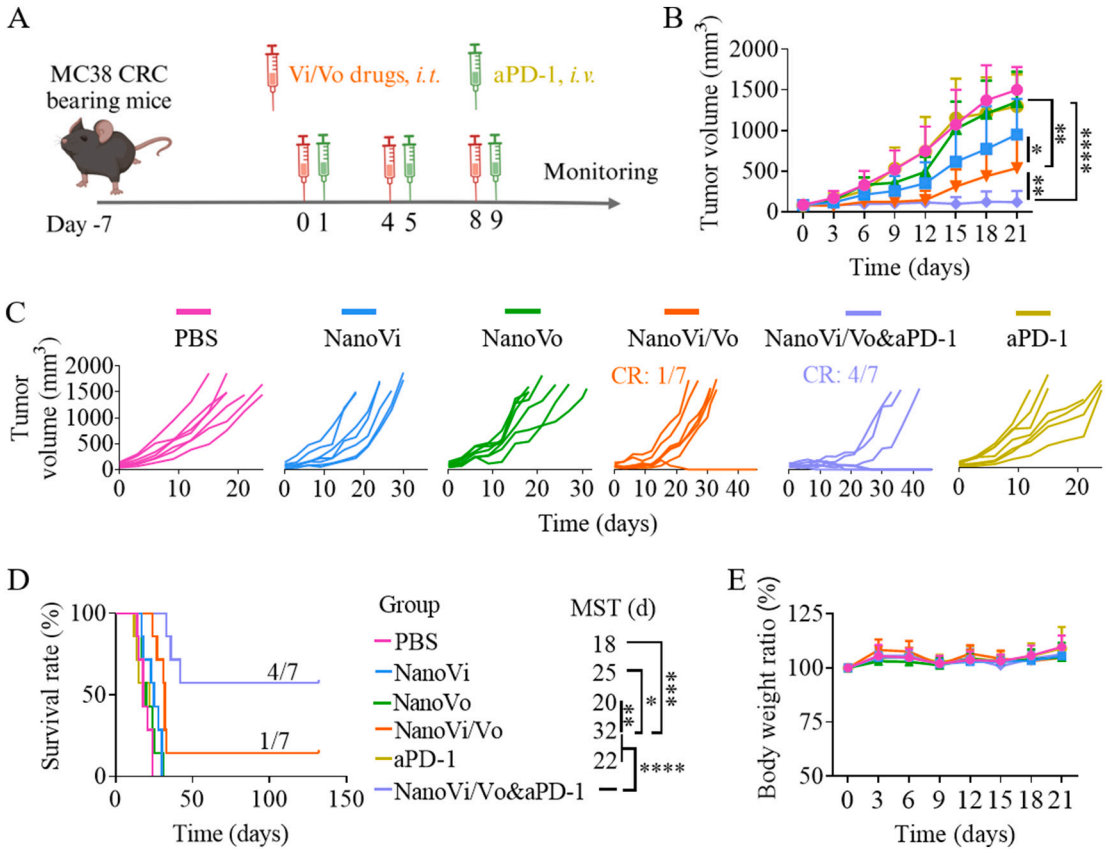

Fig. 5. In vivo therapeutic effects of NanoVi/Vo in combination with aPD-1 in a subcutaneous MC38 CRC model. (A) Model establishment and treatment schedule. (B) Average and (C) individual tumor growth curves following different treatments ($n = 7$). (D) Survival curves and body weight changes of the mice in the different groups (n = 7). *$p < 0.05$, **$p < 0.01$, ***$p < 0.001$, ****$p < 0.0001$.

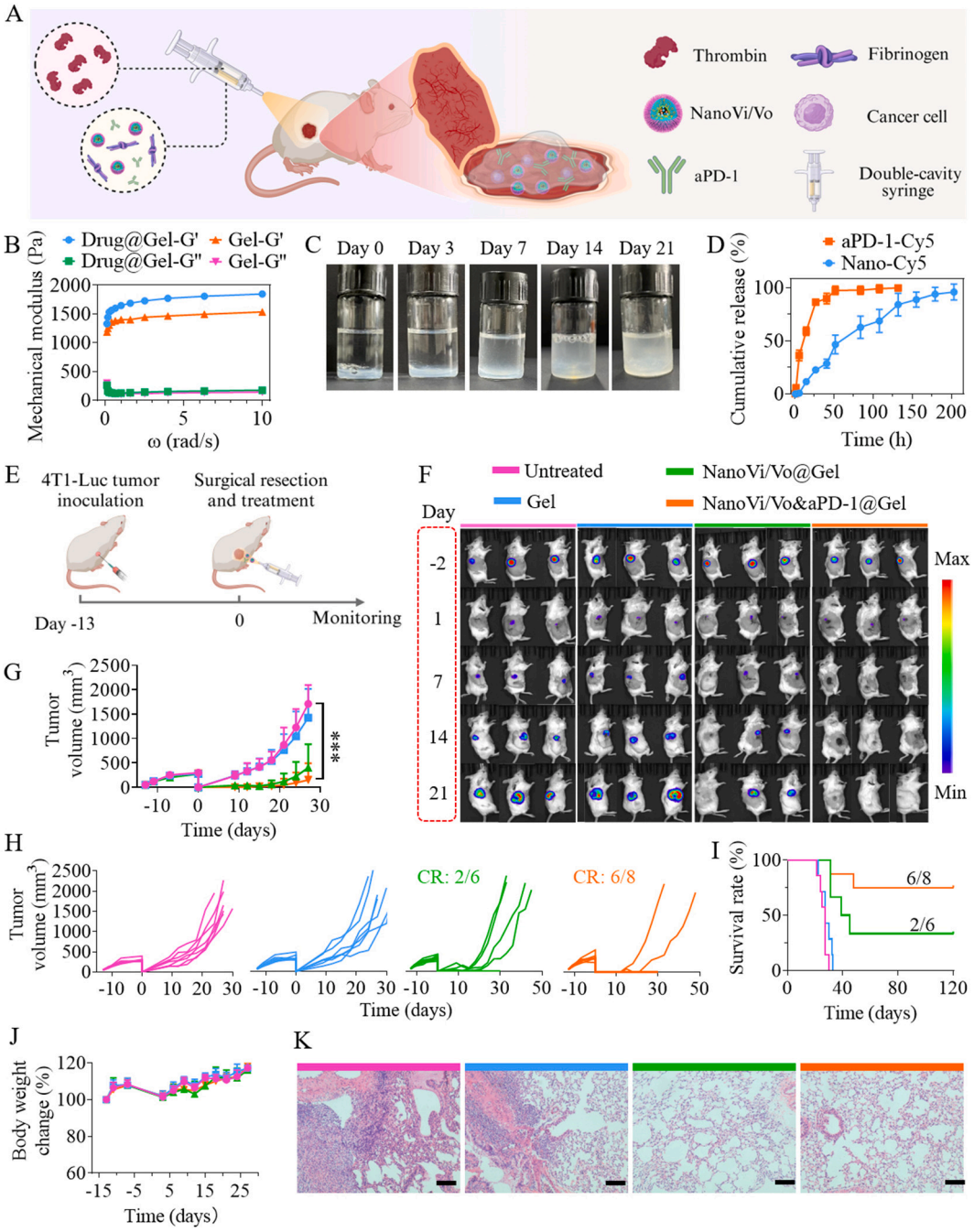

Fig. 6. Preparation of NanoVi/Vo&aPD-1@Gel for the treatment of a postoperative 4T1-Luc TNBC model. (A) Schematic showing the postsurgical treatment with NanoVi/Vo&aPD-1@Gel. (B) Storage modulus (G') and loss modulus (G") of NanoVi/Vo&aPD-1@Gel (Drug@Gel) and Gel determined by a rheometer. (C) In vitro degradation of NanoVi/Vo&aPD-1@Gel in 1× PBS. (D) Cumulative release of aPD-1-Cy5 and Nano-Cy5 from fibrin gel in PBS ($n = 3$). (E) Treatment schedule. (F) Representative bioluminescence images of the mice in the untreated, Gel, NanoVi/Vo@Gel, and NanoVi/Vo&aPD-1@Gel groups. (G) Average tumor and (H) individual tumor growth curves, (I) survival curves and (J) body weight changes of the mice after different treatments ($n = 6$ or 8). ***$p < 0.001$. (K) H&E-stained images of lungs from different groups. Scale bars: 100 μm.

30 days (Fig. 6I). Although body weight decreased slightly as a result of surgery, it was not influenced by the treatment (Fig. 6J). Lung metastasis frequently occurs in TNBC patients following surgical resection [52–54]. H&E-stained images and ex vivo bioluminescence images collectively revealed that there was no obvious tumor invasion in the lungs of cured mice even on day 120 after treatment with either NanoVi/Vo@Gel or NanoVi/Vo&aPD-1@Gel (Fig. 6K, S14). However, the mice in the untreated and Gel groups presented apparent lung metastasis on day 27 after resection.

3. Conclusion

We have demonstrated that polymersomal vincristine/volasertib (NanoVi/Vo) based ICD nanoinducer synergistically induce ICD in cancer cells and enhance immunotherapy in different cancer models. NanoVi/Vo effectively stimulates DC maturation, promotes T cell activation, and enhances the secretion of proinflammatory cytokines, thereby reversing the immunosuppressive TME. NanoVi/Vo remarkably potentiated immunotherapy in subcutaneous 4T1 and MC38 cancer models, which, in combination with aPD-1, led to complete remission in

> 57 % of the mice. Moreover, fibrin gel-mediated local delivery of NanoVi/Vo and aPD-1 completely inhibited tumor recurrence and metastasis in 75 % of post-surgery 4T1-bearing mice. Collectively, these findings confirm that NanoVi/Vo is a promising ICD inducer for enhancing immunotherapy in solid tumors.

4. Materials and methods

4.1. Preparation and characterization of NanoVi/Vo

PEG-P(TMC-DTC)-Ac-KD_{10} (5.0-(15.0-2.0)-1.3 kg/mol) was utilized to prepare disulfide-crosslinked chimeric polymersomes via one-step self-assembly, during which Vi and Vo could be efficiently loaded into the hydrophilic cavity via electrostatic interactions. First, Vi and Vo were dissolved in water and DMSO at concentrations of 5 and 20 mg/mL, respectively. Then, 1.0 mL of Vo solution was mixed with 2.5 mL of a DMSO solution of PEG-P(TMC-DTC)-Ac-KD_{10} (40 mg/mL) and injected into a solution containing 21.5 mL of HEPES buffer (5 mM, pH 6.8) and 0.4 mL of Vi solution under stirring. Afterwards, the suspension was dialyzed against HEPES buffer (5 mM, pH 7.4) for six hours to yield NanoVi/Vo. Single-drug polymersomes, NanoVi and NanoVo, were prepared similarly. The size, size distribution and stability of NanoVi/Vo were determined via DLS. The drug retention of NanoVi/Vo during long-term storage and the drug release of NanoVi/Vo from fibrin gel were determined via HPLC. The morphology of NanoVi/Vo after long-term storage was observed via transmission electron microscopy (TEM, FEI Tecnai G220).

4.2. Synergistic antitumor effect of NanoVi/Vo in vitro

The antitumor effects of NanoVi/Vo in 4T1 triple-negative breast cancer (TNBC) cells as well as MC38 and CT26 colon cancer cells were first evaluated via the MTT assay. The cells seeded in 96-well plates ($1.5–3 \times 10^3$/well) were incubated with NanoVi, NanoVo and NanoVi/Vo at Vi and Vo concentrations ranging from 0.1 to 100 ng/mL and 1 to 200 ng/mL, respectively ($n = 6$). After 72 h of incubation, 10 μL of MTT solution in PBS (5 mg/mL) was added to each well and further incubated for 4 h. Then, the cell medium was aspirated, and 150 μL of DMSO was added to dissolve the purple formazan produced by living cells. The absorbance of each well at a wavelength of 570 nm was measured via a Multiskan FC microplate, and the cell viability was subsequently calculated. Dose-response inhibition curves were fitted with GraphPad Prism 8.0.0 to determine the IC_{50} values. The synergy of Vi and Vo was evaluated by calculating the CI values via the following formulation:

$$CI = \frac{IC_{50} \text{ of Vi in NanoVi/Vo}}{IC_{50} \text{ of NanoVi}} + \frac{IC_{50} \text{ of Vo in NanoVi/Vo}}{IC_{50} \text{ of NanoVo}}$$

CI values indicate the following effects: $CI < 1$ indicates a synergistic effect, $CI = 1$ indicates an additive effect, and $CI > 1$ suggests an antagonistic effect.

An Annexin V-APC/7-AAD apoptosis kit was further used to evaluate the proapoptotic ability of NanoVi/Vo in 4T1 and MC38 cells. The cells were seeded in 12-well plates (1×10^4/well) and incubated with NanoVi, NanoVo or NanoVi/Vo (Vi: 3 ng/mL; Vo: 72 ng/mL) for 48 h ($n = 3$). After washing, trypsinization and centrifugation, the cells were resuspended in 500 μL of binding buffer, stained with 5 μL of Annexin-APC and 10 μL of 7-AAD for 5 min at 25 °C, and analyzed via flow cytometry. The data were analyzed with FlowJo software.

4.3. NanoVi/Vo-induced ICD effect

The ICD effects were studied in 4T1 and MC38 cells via the determination of typical ICD markers, including CRT, ATP and HMGB1. Cells seeded in 12-well plates (1×10^5/well) were incubated with NanoVi, NanoVo or NanoVi/Vo (Vi: 3 ng/mL, Vo: 72 ng/mL) for 48 h, with PBS used as a control ($n = 3$). Afterwards, the culture medium was collected to determine ATP and HMGB1 levels via an enhanced ATP assay kit and a mouse HMGB1 ELISA kit. The cells were collected and sequentially incubated with aCRT for 1 h and Alexa Fluor 647-conjugated secondary antibody for 30 min, followed by flow cytometry analysis. The data were analyzed via FlowJo software to determine CRT expression.

4.4. Maturation of BMDCs stimulated with NanoVi/Vo-induced ICD

The effects of NanoVi/Vo-induced ICD on BMDC maturation were studied via flow cytometry. First, 4T1 and MC38 cells seeded in 12-well plates (1×10^5/well) were incubated with NanoVi, NanoVo or NanoVi/Vo (Vi: 3 ng/mL, Vo: 72 ng/mL) for 24 h ($n = 3$). Then, BMDCs (1×10^6/well) extracted from C57BL/6J female mice were added to each well and cocultured for another 24 h. Culture medium was collected to detect cytokines, such as IL-6 and TNF-α, via a mouse IL-6 ELISA kit and a mouse TNF-α ELISA kit. The cells were collected and sequentially stained with anti-CD11c-FITC, anti-CD80-APC and anti-CD86-PE antibodies, followed by flow cytometry analysis. Mature BMDCs ($CD11c^+CD80^+CD86^+$ mDCs) were analyzed and quantified via FlowJo software.

4.5. Influence of NanoVi/Vo on the extracellular PD-L1 expression of tumor cells

The influence of NanoVi/Vo on the PD-L1 level on the cell surface was studied in 4T1 and MC38 cells, with NanoVi and NanoVo used as controls ($n = 3$). The cells were seeded in 12-well plates (1×10^5/well) and treated with various concentrations of NanoVi, NanoVo or NanoVi/Vo for 24 h or 48 h. Then, the cells were collected and washed by centrifugation, blocked with a CD16/32 antibody, and stained with anti-mouse CD274-PE for flow cytometry analysis. The data were analyzed with FlowJo software.

4.6. Tumoral retention of NanoVi/Vo

All animal procedures were performed in accordance with the Guidelines for Care and Use of Laboratory Animals of Soochow University (China) and approved by the Animal Ethics Committee of Soochow University. A murine 4T1 subcutaneous mouse model, established by injecting 50 μL of 4T1 cell suspension (5×10^5/mouse) with 20 vol% Matrigel subcutaneously into the right flank of female BALB/c mice, was used to evaluate the retention of NanoVi/Vo at the tumor site. Nano-Cy5 was prepared via the assembly of PEG-P(TMC-DTC)-Ac-KD_{10} and PEG-P(TMC-DTC)-Cy5 to monitor tumoral retention, with free Cy5 serving as a control. When the tumors grew to an average volume of approximately 150–200 mm^3, the mice were locally depilated, and 50 μL of Nano-Cy5 or free Cy5 (Cy5: 0.4 μg per mouse) was injected intratumorally. The mice were monitored via an IVIS imaging system at 0 h, 4 h, and 8 h post-injection.

4.7. In vivo antitumor effects of NanoVi/Vo in combination with aPD-1

Murine 4T1 and MC38 subcutaneous mouse models were established by injecting 50 μL of 4T1 (2×10^5/mouse) or MC38 (1×10^6/mouse) cell suspensions with 20 vol% Matrigel subcutaneously into the right flank of BALB/c mice (6–8 weeks, female) to evaluate the antitumor effects. When the tumors grew to an average volume of approximately 50–100 mm^3 at approximately 7 days after inoculation (designated day 0), the mice were randomly divided into six groups ($n = 8$ for the 4T1 model and $n = 6$ for the MC38 model): PBS, NanoVi, NanoVo, aPD-1, NanoVi/Vo and NanoVi/Vo&aPD-1. On days 0, 4 and 8, the polymersomal formulations were intratumorally injected at Vi/Vo dosages of 0.25/6 mg/kg, and aPD-1 was intravenously injected at a dosage of 1 mg/kg one day later (days 1, 5 and 9). The tumor volume, weight and survival of the mice were monitored. The deaths of the mice were recorded when the tumors exceeded 1500 mm^3 or at the time of natural

death.

4.8. Memory T-cell and immune cell infiltration analysis in vivo

To confirm the immune memory effect, 3 mice in the NanoVi/Vo group and 5 mice in the NanoVi/Vo&aPD-1group, which had been successfully cured, were rechallenged with 2×10^5 4T1 cells on the contralateral side on day 76. The tumors were measured with a caliper until day 14 post rechallenge. Then, the spleens and peripheral blood were harvested to analyze the proportions of Tregs, Tem (effector memory T cells, $CD62L^-CD44^+$) and Tcm (central memory T cells, $CD62L^+CD44^+$) via flow cytometry.

A subcutaneous 4T1 model was further established to analyze immune cell infiltration in vivo. When the average tumor volume reached 50–100 mm^3, the mice were randomly divided into five groups (n = 6) to receive PBS, NanoVi, NanoVo, NanoVi/Vo or NanoVi/Vo&aPD-1. The polymersomal formulations were intratumorally injected on days 0 and 4, and aPD-1 was intravenously injected on days 1 and 5. The drug dosages used were the same as those used in the antitumor studies. Six hours after the last injection of aPD-1, mouse plasma was collected to quantify the concentrations of TNF-α and IL-6. One day after the last injection, five mice from each group were sacrificed, and the tumors and spleens were collected, weighed and ground into single-cell suspensions to analyze the numbers of $CD8^+$ T, $CD4^+$ T and Treg cells via flow cytometry. Another mouse in each group was sacrificed to collect the major organs and tumors, which were then stained with hematoxylin and eosin (H&E) for histological analysis. The tumor slices were also stained with different antibodies to identify CRT^+ tumor cells, $CD11c^+CD86^+$ cells and $CD8^+$ T cells.

4.9. Preparation and characterization of NanoVi/Vo&aPD-1@Gel

A commercially available and clinically used porcine fibrin sealant kit with fibrinogen and thrombin as the main components was used to prepare drug-loaded hydrogels, thus enabling local treatment and sustained drug release in the postoperative model. Fibrinogen and thrombin were dissolved separately according to the user guide. To prepare NanoVi/Vo and aPD-1-coloaded gels, a NanoVi/Vo suspension at a polymer concentration of 40 mg/mL was first mixed with aPD-1 solution (9.67 mg/mL) and then mixed with the fibrinogen solution at a volume ratio of 1:1. The resulting mixture was further blended with thrombin solution at a volume ratio of 1:1, which can form gels in seconds and afford NanoVi/Vo&aPD-1@Gel. NanoVi/Vo@Gel was prepared similarly without the addition of aPD-1. Blank gel (Gel) was prepared by mixing the fibrinogen and thrombin solutions according to the user guide. The morphology of NanoVi/Vo&aPD-1@Gel was confirmed via FESEM. The rheological properties of NanoVi/Vo&aPD-1@Gel and Gel were measured via a rheometer. The degradation of the NanoVi/Vo&aPD-1@Gel in 1 × PBS was recorded constantly by observing the status of the gel. The cytotoxicity of the blank gel was assessed via a CCK-8 assay. To determine the release behavior of antibodies and polymersomes from the gel, aPD-1-Cy5@Gel or Nano-Cy5@Gel was immersed in PBS at 25 °C. At different time points, the supernatant was collected to determine the amount of released aPD-1-Cy5 or Nano-Cy5 via fluorescence spectrometry.

4.10. NanoVi/Vo&aPD-1@Gel-mediated immunotherapy in the postoperative 4T1-Luc model

A postoperative 4T1-Luc model was employed to further validate the efficacy of NanoVi/Vo and aPD-1 in the treatment of postsurgical tumors. 4T1-Luc cells (3×10^5/mouse) were subcutaneously inoculated into the right flank of BALB/c mice. When the tumors grew to 200–300 mm^3 at approximately 13 days after inoculation, the mice were anesthetized and locally disinfected to surgically remove ca. 99 % of the tumor volume, leaving approximately 1 % residual tumor tissue. Gel, NanoVi/Vo@Gel and NanoVi/Vo&aPD-1@Gel (Vi/Vo: 0.25/6 mg/kg; aPD-1: 1 mg/kg; Gel: 200 μL/mouse) were dripped into the postoperative cavity, followed by wound suturing. One group of untreated mice served as a control. Tumor recurrence and growth were monitored via bioluminescence imaging via an In Vivo IVIS Spectrum Imaging System. To minimize potential interference from the fur, the hair surrounding the tumor was meticulously removed via depilatory cream prior to imaging. The tumor volume, weight and survival of the mice were continually monitored. On day 120, one cured mouse from the NanoVi/Vo@Gel or NanoVi/Vo&aPD-1@Gel group was sacrificed, and the lungs were harvested for ex vivo imaging and H&E staining. The lungs isolated from the untreated or Gel groups at the experimental endpoint were used as controls. The deaths of the mice were recorded when the tumors exceeded 1500 mm^3 or at the time of natural death.

4.11. Statistical analysis

The data are presented as the means ± standard deviations. Significant differences among groups were determined via one-way ANOVA with Tukey's multiple comparison test via GraphPad Prism 8.0.0 software. The survival of the mice was analyzed via the Kaplan–Meier method and compared via a log-rank (Mantel–Cox) test. $^*p < 0.05$, $^{**}p < 0.01$, $^{***}p < 0.001$, $^{****}p < 0.0001$.

CRediT authorship contribution statement

Yan Zhao: Writing – original draft, Methodology, Investigation, Formal analysis, Data curation. **Li Cao:** Resources, Methodology, Investigation. **Songsong Zhao:** Resources, Methodology. **Zhenzhen Zhai:** Investigation, Formal analysis. **Xueling Tang:** Methodology, Formal analysis. **Lin Chen:** Investigation, Formal analysis. **Huanli Sun:** Writing – review & editing, Supervision, Project administration, Funding acquisition, Conceptualization. **Zhiyuan Zhong:** Writing – review & editing, Supervision, Project administration, Funding acquisition, Conceptualization.

Declaration of competing interest

The authors declare that they have no known competing financial interests or personal relationships that could have appeared to influence the work reported in this paper.

Acknowledgements

This work was supported by the National Natural Science Foundation of China (52473264, 52273251 and 52233007). The schemes in the figures were created with BioRender.com.

Appendix A. Supplementary data

Supplementary data to this article can be found online at https://doi.org/10.1016/j.cej.2025.164657.

Data availability

Data will be made available on request.

References

[1] A. Fenis, O. Demaria, L. Gauthier, E. Vivier, E. Narni-Mancinelli, New immune cell engagers for cancer immunotherapy, Nat. Rev. Immunol. 24 (2024) 471–486.
[2] L. Kraehenbuehl, C.-H. Weng, S. Eghbali, J.D. Wolchok, T. Merghoub, Enhancing immunotherapy in cancer by targeting emerging immunomodulatory pathways, Nat. Rev. Clin. Oncol. 19 (2022) 37–50.
[3] M.U. Farooq, C.H. Lawrie, N.-N. Deng, Engineering nanoparticles for cancer immunotherapy: current achievements, key considerations and future perspectives, Chem. Eng. J. 486 (2024) 150356.

[4] Y. Song, L. Teng, Y. Chen, C.-M. Dong, Glycopolypeptide coordinated nanovaccine: fabrication, characterization, and antitumor immune response, Chem. Bio. Eng. 1 (2024) 633–646.
[5] G. Oliveira, C.J. Wu, Dynamics and specificities of T cells in cancer immunotherapy, Nat. Rev. Cancer 23 (2023) 295–316.
[6] B. Wang, J. Zhou, R. Li, D. Tang, Z. Cao, C. Xu, H. Xiao, Activating CD8+ T cells by Pt(IV) prodrug-based nanomedicine and aPD-L1 antibody for enhanced cancer immunotherapy, Adv. Mater. 36 (2024) 2311640.
[7] R. Li, Z. Chen, J. Li, Z. Dai, Y. Yu, Nano-drug delivery systems for T cell-based immunotherapy, Nano Today 46 (2022) 101621.
[8] D.J. Irvine, E.L. Dane, Enhancing cancer immunotherapy with nanomedicine, Nat. Rev. Immunol. 20 (2020) 321–334.
[9] S.P. Kubli, T. Berger, D.V. Araujo, L.L. Siu, T.W. Mak, Beyond immune checkpoint blockade: emerging immunological strategies, Nat. Rev. Drug Discov. 20 (2021) 899–919.
[10] S.W. Linderman, L. DeRidder, L. Sanjurjo, M.B. Foote, M.J. Alonso, A.R. Kirtane, R. Langer, G. Traverso, Enhancing immunotherapy with tumour-responsive nanomaterials, Nat. Rev. Clin. Oncol. 22 (2025) 262–282.
[11] Y. Jin, Y. Huang, H. Ren, H. Huang, C. Lai, W. Wang, Z. Tong, H. Zhang, W. Wu, C. Liu, X. Bao, W. Fang, H. Li, P. Zhao, X. Dai, Nano-enhanced immunotherapy: targeting the immunosuppressive tumor microenvironment, Biomaterials 305 (2024) 122463.
[12] F. Ghiringhelli, C. Rébé, Using immunogenic cell death to improve anticancer efficacy of immune checkpoint inhibitors: from basic science to clinical application, Immunol. Rev. 321 (2024) 335–349.
[13] L. Galluzzi, E. Guilbaud, D. Schmidt, G. Kroemer, F.M. Marincola, Targeting immunogenic cell stress and death for cancer therapy, Nat. Rev. Drug Discov. 23 (2024) 445–460.
[14] F. Shi, X. Huang, Z. Hong, N. Lu, X. Huang, L. Liu, T. Liang, X. Bai, Improvement strategy for immune checkpoint blockade: a focus on the combination with immunogenic cell death inducers, Cancer Lett. 562 (2023) 216167.
[15] N. Bie, T. Yong, Z. Wei, Q. Liang, X. Zhang, S. Li, X. Li, J. Li, L. Gan, X. Yang, Tumor-repopulating cell-derived microparticles elicit cascade amplification of chemotherapy-induced antitumor immunity to boost anti-PD-1 therapy, Sig. Transduct. Target. Ther. 8 (2023) 408.
[16] M. He, Y. Song, W. Xu, X. Zhang, C.-M. Dong, Four birds with one stone: a multifunctional polypeptide nanocomposite to unify ferroptosis, nitric oxide, and photothermia for amplifying antitumor immunity, Adv. Funct. Mater. 33 (2023) 2304216.
[17] L. Galluzzi, J. Humeau, A. Buqué, L. Zitvogel, G. Kroemer, Immunostimulation with chemotherapy in the era of immune checkpoint inhibitors, Nat. Rev. Clin. Oncol. 17 (2020) 725–741.
[18] Z. Li, X. Lai, S. Fu, L. Ren, H. Cai, H. Zhang, Z. Gu, X. Ma, K. Luo, Immunogenic cell death activates the tumor immune microenvironment to boost the immunotherapy efficiency, Adv. Sci. 9 (2022) 2201734.
[19] G. Petroni, A. Buqué, L. Zitvogel, G. Kroemer, L. Galluzzi, Immunomodulation by targeted anticancer agents, Cancer Cell 39 (2021) 310–345.
[20] W. Pan, F. Gao, H. Wang, Y. Guo, M. Rafiq, H. Cong, Y. Shen, B. Yu, Synergistic induction of immunogenic cell death by icaritin, JQ1, and doxorubicin to enhance immunotherapy in hepatocellular carcinoma, Chem. Eng. J. 508 (2025) 160987.
[21] M. Yang, C. Zhang, R. Wang, X. Wu, H. Li, J. Yoon, Cancer immunotherapy elicited by immunogenic cell death based on smart nanomaterials, Small Methods 7 (2023) 2201381.
[22] J.L. Peng, S.Y. Li, H.H. Ti, Sensitize tumor immunotherapy: immunogenic cell death inducing nanosystems, Int. J. Nanomedicine 19 (2024) 5895–5930.
[23] J. Zhang, L. Zhang, J. Wang, L. Ouyang, Y. Wang, Polo-like kinase 1 inhibitors in human cancer therapy: development and therapeutic potential, J. Med. Chem. 65 (2022) 10133–10160.
[24] M. Reda, W. Ngamcherdtrakul, M.A. Nelson, N. Siriwon, R. Wang, H.Y. Zaidan, D. S. Bejan, S. Reda, N.H. Hoang, N.A. Crumrine, J.P.C. Rehwaldt, A. Bindal, G. B. Mills, J.W. Gray, W. Yantasee, Development of a nanoparticle-based immunotherapy targeting PD-L1 and PLK1 for lung cancer treatment, Nat. Commun. 13 (2022) 4261.
[25] S. Iliaki, R. Beyaert, I.S. Afonina, Polo-like kinase 1 (PLK1) signaling in cancer and beyond, Biochem. Pharmacol. 193 (2021) 114747.
[26] R.E.A. Gutteridge, M.A. Ndiaye, X. Liu, N. Ahmad, PLK1 inhibitors in cancer therapy: from laboratory to clinics, Mol. Cancer Ther. 15 (2016) 1427–1435.
[27] J. Zhou, Q. Yang, L. Lu, Z. Tuo, Z. Shou, J. Cheng, PLK1 inhibition induces immunogenic cell death and enhances immunity against NSCLC, Int. J. Med. Sci. 18 (2021) 3516–3525.
[28] L.M. Weiß, M. Hugle, S. Romero, S. Fulda, Synergistic induction of apoptosis by a polo-like kinase 1 inhibitor and microtubule-interfering drugs in Ewing sarcoma cells, Int. J. Cancer 138 (2016) 497–506.
[29] N. Yu, Y. Zhang, J. Li, W. Gu, S. Yue, B. Li, F. Meng, H. Sun, R. Haag, J. Yuan, Z. Zhong, Daratumumab immunopolymersome-enabled safe and CD38-targeted chemotherapy and depletion of multiple myeloma, Adv. Mater. 33 (2021) 2007787.
[30] A. Kothari, W.N. Hittelman, T.C. Chambers, Cell cycle-dependent mechanisms underlie vincristine-induced death of primary acute lymphoblastic leukemia cells, Cancer Res. 76 (2016) 3553–3561.
[31] S. Yue, J. An, Y. Zhang, J. Li, C. Zhao, J. Liu, L. Liang, H. Sun, Y. Xu, Z. Zhong, Exogenous antigen upregulation empowers antibody targeted nanochemotherapy of leukemia, Adv. Mater. 35 (2023) 2209984.
[32] Y. Zhang, J. An, Y. Shao, N. Yu, S. Yue, H. Sun, J. Zhang, W. Gu, Y. Xia, J. Zhang, Y. Xu, Z. Zhong, CD38-directed vincristine nanotherapy for acute lymphoblastic leukemia, Biomacromolecules 23 (2022) 377–387.
[33] D.F. Chen, C.Y. Lei, W.F. Liu, M.Y. Shao, M.Z. Sun, J.X. Guo, J.J. Cao, P. Luo, Y. W. Luo, B.R. Yu, R.X. Wang, S. Duan, F.J. Xu, Reduction-responsive nucleic acid nanocarrier-mediated miR-22 inhibition of PI3K/AKT pathway for the treatment of patient-derived tumor xenograft osteosarcoma, Bioact. Mater. 28 (2023) 376–385.
[34] E. Pujade-Lauraine, F. Selle, B. Weber, I.L. Ray-Coquard, I. Vergote, J. Sufliarsky, J. M. Del Campo, A. Lortholary, A. Lesoin, P. Follana, G. Freyer, B. Pardo, L. Vidal, B. Tholander, L. Gladieff, M. Sassi, P. Garin-Chesa, S. Nazabadioko, K. Marzin, K. Pilz, F. Joly, Volasertib versus chemotherapy in platinum-resistant or -refractory ovarian cancer: a randomized phase ii groupe des investigateurs nationaux pour l'etude des cancers de l'ovaire study, J. Clin. Oncol. 34 (2016) 706–713.
[35] J. Du, S. Yue, C. Li, J. Li, S. Zhao, Y. Dong, Y. Zhang, R. Cheng, H. Sun, Z. Zhong, Exogenous CD38 upregulation enables high-efficacy dually cascade targeted molecular therapy of leukemia, Nano Today 50 (2023) 101872.
[36] P. Liu, L.W. Zhao, J. Pol, S. Levesque, A. Petrazzuolo, C. Pfirschke, C. Engblom, S. Rickelt, T. Yamazaki, K. Iribarren, L. Senovilla, L. Bezu, E. Vacchelli, V. Sica, A. Melis, T. Martin, X. Lin, H. Yang, Q.Q. Li, J.F. Chen, S. Durand, F. Aprahamian, D. Lefevre, S. Broutin, A. Paci, A. Bongers, V. Minard-Colin, E. Tartour, L. Zitvogel, L. Apetoh, Y.T. Ma, M.J. Pittet, O. Kepp, G. Kroemer, Crizotinib-induced immunogenic cell death in non-small cell lung cancer, Nat. Commun. 10 (2019) 1486.
[37] A. Gulla, E. Morelli, M.K. Samur, C. Botta, T. Hideshima, G. Bianchi, M. Fulciniti, S. Malvestiti, R. Prabhala, S. Talluri, Y.T. Tai, K. Wen, P.G. Richardson, R. D. Carrasco, D. Chauhan, N.C. Munshi, K. Anderson, Bortezomib induces anti-multiple myeloma immune response mediated by cGAS/STING pathway activation, type I interferon secretion, and immunogenic cell death: clinical application, Blood 136 (2020) 7–8.
[38] H. Xiao, X.X. Li, S.M. Liang, S.G. Yang, S.S. Han, J.S. Huang, X.T. Shuai, J. Ren, Dual-responsive nanomedicine activates programmed antitumor immunity through targeting lymphatic system, ACS Nano 18 (2024) 11070–11083.
[39] Y. He, S.Y. Wu, Y.B. Yuan, Y.C. Sun, Q.J. Ai, R.Q. Zhou, G.Z. Chai, D.W. Chen, H. Y. Hu, Remodeling tumor immunosuppression with molecularly imprinted nanoparticles to enhance immunogenic cell death for cancer immunotherapy, J. Control. Release 362 (2023) 44–57.
[40] L. Xie, G. Wang, W. Sang, J. Li, Z. Zhang, W. Li, J. Yan, Q. Zhao, Y. Dai, Phenolic immunogenic cell death nanoinducer for sensitizing tumor to PD-1 checkpoint blockade immunotherapy, Biomaterials 269 (2021) 120638.
[41] H.J. Hwang, D. Kang, J. Shin, J. Jung, S. Ko, K.H. Jung, S.-S. Hong, J.E. Park, M. J. Oh, H.J. An, W.-H. Yang, Y.-G. Ko, J.-H. Cha, J.-S. Lee, Therapy-induced senescent cancer cells contribute to cancer progression by promoting ribophorin 1-dependent PD-L1 upregulation, Nat. Commun. 16 (2025) 353.
[42] J. Xiang, K. Liu, H. Xu, Z. Zhao, Y. Piao, S. Shao, J. Tang, Y. Shen, Z. Zhou, Dual synergistic tumor-specific polymeric nanoparticles for efficient chemo-immunotherapy, Adv. Sci. 10 (2023) 2301216.
[43] A. Hernández-Prat, A. Rodriguez-Vida, L. Cardona, M. Qin, O. Arpí-Llucià, L. Soria-Jiménez, S. Menendez, F.G. Quimis, M. Galindo, E. Arriola, M. Salido, N. Juanpere-Rodero, F. Rojo, A. Muntasell, J. Albanell, A. Rovira, J. Bellmunt, Enhancing immunotherapy through PD-L1 upregulation: the promising combination of anti-PD-L1 plus mTOR inhibitors, Mol. Oncol. 19 (2025) 151–172.
[44] S.E. Stanton, M.L. Disis, Clinical significance of tumor-infiltrating lymphocytes in breast cancer, J. Immunother. Cancer 4 (2016) 59.
[45] Z. Luo, Y. Lu, Y. Shi, M. Jiang, X. Shan, X. Li, J. Zhang, B. Qin, X. Liu, X. Guo, J. Huang, Y. Liu, S. Wang, Q. Li, L. Luo, J. You, Neutrophil hitchhiking for drug delivery to the bone marrow, Nat. Nanotechnol. 18 (2023) 647–656.
[46] S. Parveen, S. Siddharth, L.S. Cheung, A. Kumar, J. Shen, J.R. Murphy, D. Sharma, W.R. Bishai, Therapeutic targeting with DABIL-4 depletes myeloid suppressor cells in 4T1 triple-negative breast cancer model, Mol. Oncol. 15 (2021) 1330–1344.
[47] Q. Chen, C. Wang, X. Zhang, G. Chen, Q. Hu, H. Li, J. Wang, D. Wen, Y. Zhang, Y. Lu, G. Yang, C. Jiang, J. Wang, G. Dotti, Z. Gu, In situ sprayed bioresponsive immunotherapeutic gel for post-surgical cancer treatment, Nat. Nanotechnol. 14 (2019) 89–97.
[48] Y. Qin, G. Wang, L. Chen, Y. Sun, J. Yang, Y. Piao, Y. Shen, Z. Zhou, High-throughput screening of surface engineered cyanine nanodots for active transport of therapeutic antibodies into solid tumor, Adv. Mater. 36 (2024) 2302292.
[49] Q.S. Hu, Y. Nie, J. Xiang, J.W. Xie, H.B. Si, D.H. Li, S.Y. Zhang, M. Li, S.S. Huang, Injectable sodium alginate hydrogel loaded with plant polyphenol-functionalized silver nanoparticles for bacteria-infected wound healing, Int. J. Biol. Macromol. 234 (2023) 123691.
[50] L. Mao, L. Wang, M. Zhang, M.W. Ullah, L. Liu, W. Zhao, Y. Li, A.A.Q. Ahmed, H. Cheng, Z. Shi, G. Yang, In situ synthesized selenium nanoparticles-decorated bacterial cellulose/gelatin hydrogel with enhanced antibacterial, antioxidant, and anti-inflammatory capabilities for facilitating skin wound healing, Adv. Healthc. Mater. 10 (2021) 2100402.
[51] X. Xue, H. Zhang, H. Liu, S. Wang, J. Li, Q. Zhou, X. Chen, X. Ren, Y. Jing, Y. Deng, Z. Geng, X. Wang, J. Su, Rational design of multifunctional CuS nanoparticle-PEG composite soft hydrogel-coated 3D hard polycaprolactone scaffolds for efficient bone regeneration, Adv. Funct. Mater. 32 (2022) 2202470.
[52] G.D. Xie, H.Y. Yang, D. Ma, Y.H. Sun, H.Q. Chen, X. Hu, Y.Z. Jiang, Z.M. Shao, Integration of whole-genome sequencing and functional screening identifies a

prognostic signature for lung metastasis in triple-negative breast cancer, Int. J. Cancer 145 (2019) 2850–2860.
[53] P. Yu, Y.B. Han, L.L. Meng, Z.Y. Tang, Z.W. Jin, Z.Z. Zhang, Y.J. Zhou, J. Luo, J. G. Luo, C. Han, C. Zhang, L.Y. Kong, The incorporation of acetylated LAP-TGF-β1 proteins into exosomes promotes TNBC cell dissemination in lung micro-metastasis, Mol. Cancer 23 (2024) 82.
[54] B. Guo, Y. Qu, Y. Sun, S. Zhao, J. Yuan, P. Zhang, Z. Zhong, F. Meng, Co-delivery of gemcitabine and paclitaxel plus NanoCpG empowers chemoimmunotherapy of postoperative “cold” triple-negative breast cancer, Bioact. Mater. 25 (2023) 61–72.